Preprints of the 19th World Congress
The International Federation of Automatic Control
Cape Town, South Africa. August 24-29, 2014

Flight Test Results for Circular Path Following by Model Predictive Control

Yoshiro Hamada * **Taro Tsukamoto** * **Shinji Ishimoto** *

* *Japan Aerospace Exploration Agency, Mitaka, Tokyo 181-0015 Japan (e-mail: {hamada.yoshiro}{tsukamoto.taro}{ishimoto.shinji}@jaxa.jp).*

Abstract: This paper describes a novel lateral guidance law of an unmanned aerial vehicle using model predictive control and shows its flight test results. The guidance law is accompanied with an extended Kalman filter which estimates steady wind velocities in order to follow a pre-specified reference path defined in the ground-fixed coordinate system. A small scale research vehicle, developed by Japan Aerospace Exploration Agency, is used for flight tests and the results show the proposed system's high guidance performance.

1. INTRODUCTION

Japan Aerospace Exploration Agency (JAXA) has been carrying out research activities for developing unmanned orbital spaceplanes and related unmanned aerial vehicles (UAVs) for decades (Shirouzu et al. [2001],NAL/NASDA HSFD1 Team [2004],NAL/NASDA HOPE Team [2005]). One of the key technologies for these issues is precise guidance with robustness against aerodynamic change. When a spaceplane comes back to the earth, it needs to land on a runway automatically. In case of emergency, "abort mode" is activated and a spaceplane is required to fly along a pre-specified path called "HAC" (Heading Alignment Cylinder) to reduce its potential energy before landing on an emergency landing site (Moore [1991]). Since a spaceplane flies from Earth orbit to a low altitude and therefore its aerodynamic characteristics change drastically, a guidance system that covers wide flight envelopes is indispensable.

Conventional guidance systems for spaceplanes such as the Space Shuttle used gain scheduling techniques along some pre-set trajectories. On the other hand, model predictive control (MPC) technique is one of the potential candidates for the future guidance system. MPC uses a plant model to be controlled in order to yield the optimal command by performing finite horizon optimization onboard (Maciejowski [2002]). If nonlinear spaceplane models along its flight path are all available, a guidance system with these models can cover wider flight envelopes by nonlinear MPC algorithm and can provide great flexibility in case of emergency. In addition, since MPC solves optimization problem onboard for each calculation step, precise guidance can also be expected.

This paper proposes a novel lateral guidance law using nonlinear MPC and demonstrates its effectiveness by flight tests using a small UAV. Although the goal of the research is the precise and robust guidance system for a spaceplane, this paper reports an early study of the guidance system and therefore limits its scope to a small UAV's lateral guidance system. The proposed system also utilizes an extended Kalman filter for steady wind velocity estimation in order to eliminate discrepancy between a runway coordinate, which is used to define a reference path to be followed, and a wind axis system, which is used in guidance and control of a vehicle. The results of flight tests for circular path following, which were conducted in 2012 using the small scale research vehicle (SSRV) developed by JAXA, are provided to show effectiveness of the proposed guidance system.

Fig. 1. Small Scale Research Vehicle (SSRV).

2. SSRV: SMALL SCALE RESEARCH VEHICLE

Fig. 1 shows the small unmanned aerial vehicle "SSRV" used in the flight tests. It is developed by JAXA and the major objective of development is to conduct flight experiments of challenging control methods more frequently with lower cost compared with large scale experimental aircrafts. SSRV is a radio-controlled unmaned aircraft with the full length of 2.6m, the wing span of 4.2m and the weight of 33kg. It has an onboard flight control system for automatic control with Micro-GAIA (GPS Aided Inertial Avionics), which is a Micro-GPS/INS integrated navigation system. The onboard CPU board is Advantech PCM-3370F-J0A1E PC/104-Plus CPU module with ULV Intel® Celeron® 400MHz Fanless and 512MB SDRAM.

3. LATERAL GUIDANCE LAW

This section describes the lateral guidance law of SSRV used in the flight tests. The designed guidance law consists of nonlinear MPC using C/GMRES method proposed in Ohtsuka [2004] and an extended Kalman filter for steady wind velocity estimation.

The longitudinal guidance, altitude control and attitude control systems are out of scope here, which are designed based on nonlinear dynamic inversion in Kawaguchi and Miyazawa [2008] with disturbance observer.

3.1 Lateral Motion of SSRV

The lateral equations of motion of SSRV are described in the following form:

$$\dot{x} = V_T \cos\chi + W_x, \tag{1}$$
$$\dot{y} = V_T \sin\chi + W_y, \tag{2}$$
$$\dot{\chi} = \frac{1}{mV_T}(L + T\sin\alpha)\sin\sigma, \tag{3}$$

where

x:	x position in the runway coordinate
y:	y position in the runway coordinate
χ:	azimuth angle (calculated using the true airspeed)
W_x:	wind velocity along x axis in the runway coordinate
W_y:	wind velocity along y axis in the runway coordinate
V_T:	true airspeed
α:	angle of attack
σ:	angle of bank
m:	mass of SSRV
L:	lift (defined in the wind axis system)
T:	engine thrust

To simplify the discussion, the longitudinal guidance and attitude control are supposed to be fulfilled appropriately and level flight is achieved. Then the following equilibrium condition holds:

$$(L + T\sin\alpha)\cos\sigma = mg,$$

where g is the gravitational constant. Consequently (3) becomes

$$\dot{\chi} = \frac{g}{V_T}\tan\sigma. \tag{4}$$

3.2 Guidance law using MPC

In the SSRV flight control system, one of the inputs of the attitude control system is the bank angle command σ_c. Thus the lateral guidance law in this paper is designed so that it yields the bank angle command σ_c that enables SSRV to follow the desired path.

Nonlinear MPC by C/GMRES method (Ohtsuka [2004])
The nonlinear system, equality constraints and the performance index J are defined respectively by

$$\begin{aligned}
&\dot{\boldsymbol{x}}(t) = \boldsymbol{f}(\boldsymbol{x}(t), \boldsymbol{u}(t)),\\
&\boldsymbol{C}(\boldsymbol{x}(t), \boldsymbol{u}(t)) = 0,\\
&J(\boldsymbol{x}_0, T_s(t), \boldsymbol{u}(t)) = \phi_J(\boldsymbol{x}^u(T_s(t); \boldsymbol{x}_0))\\
&\qquad\qquad + \int_0^{T_s} L_J(\boldsymbol{x}^u(\tau; \boldsymbol{x}_0), \boldsymbol{u}(\tau))d\tau,
\end{aligned}$$

where

$\boldsymbol{x}(t)$:	state vector
$\boldsymbol{u}(t)$:	input vector
$T_s(t)$:	duration of the prediction horizon
$\boldsymbol{x}_0$:	state vector at the beginning of the prediction horizon ($\boldsymbol{x}_0 = \boldsymbol{x}(t)$)
$\boldsymbol{C}(\cdot,\cdot)$:	equality constraints (vector-valued function)
$\phi_J(\cdot)$:	terminal cost
$L_J(\cdot,\cdot)$:	integral cost

and $\boldsymbol{x}^u(\tau; \boldsymbol{x}_0)$ in L_J denotes the state trajectory by the input function $\boldsymbol{u}(t)$ with the initial state $\boldsymbol{x}_0$.

Let H denote the Hamiltonian defined by:

$$H(\boldsymbol{x}, \lambda, \boldsymbol{u}, \mu) := L_J(\boldsymbol{x}, \boldsymbol{u}) + \lambda^T \boldsymbol{f}(\boldsymbol{x}, \boldsymbol{u}) + \mu^T \boldsymbol{C}(\boldsymbol{x}, \boldsymbol{u}),$$

where λ is the costate and μ is the Lagrange multiplier associated with the equality constraints. Then nonlinear MPC by C/GMRES method proposed in Ohtsuka [2004] is achieved for each control step as follows:

1. Divide the prediction horizon (from the current time t to $t+T_s(t)$) into N steps and discretize the optimal control problem.

$$\begin{aligned}
&\boldsymbol{x}^*_{i+1}(t) = \boldsymbol{x}^*_i(t) + \boldsymbol{f}(\boldsymbol{x}^*_i(t), \boldsymbol{u}^*_i(t))\Delta\tau(t)\\
&\boldsymbol{x}^*_0(t) = \boldsymbol{x}(t)\\
&\boldsymbol{C}(\boldsymbol{x}^*_i(t), \boldsymbol{u}^*_i(t)) = 0,\\
&\qquad (i = 0, 1, \ldots, N-1)
\end{aligned}$$

   where $\boldsymbol{x}^*_i(t)$ is the predicted state at step i in the prediction horizon, $\Delta\tau(t) := T_s(t)/N$. Then the first-order necessary conditions for the optimal control are obtained:

$$\begin{aligned}
&H^T_{\boldsymbol{u}}(\boldsymbol{x}^*_i(t), \lambda^*_{i+1}(t), \boldsymbol{u}^*_i(t), \mu^*_i(t)) = 0\\
&\lambda^*_i(t) = \lambda^*_{i+1}(t)\\
&\qquad + H^T_{\boldsymbol{x}}(\boldsymbol{x}^*_i(t), \lambda^*_{i+1}(t), \boldsymbol{u}^*_i(t), \mu^*_i(t))\Delta\tau\\
&\lambda^*_N(t) = \phi^T_{J\boldsymbol{x}}(\boldsymbol{x}^*_N(t))\\
&\qquad (i = 0, 1, \ldots, N-1)
\end{aligned}$$

2. Solve the following equation with respect to $U(t)$:

$$\begin{aligned}
&F(U(t), \boldsymbol{x}(t), t) :=\\
&\begin{bmatrix}
H^T_{\boldsymbol{u}}(\boldsymbol{x}^*_0(t), \lambda^*_1(t), \boldsymbol{u}^*_0(t), \mu^*_0(t))\\
\boldsymbol{C}(\boldsymbol{x}^*_0, \boldsymbol{u}^*_0)\\
\vdots\\
H^T_{\boldsymbol{u}}(\boldsymbol{x}^*_{N-1}(t), \lambda^*_N(t), \boldsymbol{u}^*_{N-1}(t), \mu^*_{N-1}(t))\\
\boldsymbol{C}(\boldsymbol{x}^*_{N-1}, \boldsymbol{u}^*_{N-1})
\end{bmatrix}\\
&= 0\\
&\left(U(t) := [\boldsymbol{u}^*_0(t), \mu^*_0(t), \ldots, \boldsymbol{u}^*_{N-1}(t), \mu^*_{N-1}(t)]^T\right)
\end{aligned}$$

3. Use $\boldsymbol{u}^*_0(t)$, the first term of $U(t)$, as the input to the control system $\boldsymbol{u}(t)$.

$F(U(t), \boldsymbol{x}(t), t) = 0$ in Step 2 can be efficiently solved using C/GMRES method as proposed in Ohtsuka [2004]. The initial guess of the above problem, $U(0)$, can be easily found by choosing $T_s(t)$ as a smooth function such that $T_s(0) = 0$ and $T_s(t) \to$ const.$(t \to \infty)$ (recall that the duration of the prediction horizon $T_s(t)$ is a function of

time). Then $U(0)$ is obtained as a trivial solution of a two-point boundary value problem.

In order to apply this nonlinear MPC method to each control problem, it is important how to define the equality constraints $\boldsymbol{C}(\cdot,\cdot)$ and the cost functions $\phi_J(\cdot)$ and $L_J(\cdot,\cdot)$.

Constraints and cost functions for circular path following In this paper a pre-specified reference path is limited to a circular one. The results of straight path following are shown in Hamada et al. [2014].

The system input u, that is identical to the bank command σ_c, has inequality constraints:

$$\sigma_{\min} \leq u \leq \sigma_{\max},$$

where $\sigma_{\max}$ and $\sigma_{\min}$ are maximum and minimum bank command respectively. A dummy input $\tilde{u}$ is used in order to transform inequality constraints into an equality constraint:

$$\boldsymbol{C}(\boldsymbol{x},\boldsymbol{u}) := \left(u - \frac{\sigma_{\max}+\sigma_{\min}}{2}\right)^2 + \tilde{u}^2 - \left(\frac{\sigma_{\max}-\sigma_{\min}}{2}\right)^2 = 0. \tag{5}$$

Cost functions for circular path following are defined as follows:

$$\phi_J(\boldsymbol{x}) := \{(x-x_c)^2 + (y-y_c)^2 - a^2\}^2 w_c \tag{6}$$

$$L_J(\boldsymbol{x},\boldsymbol{u}) := \{(x-x_c)^2 + (y-y_c)^2 - a^2\}^2 w_c + \frac{1}{2}u^2 w_u - \tilde{u} w_r + \{(x_c-x)\sin\chi - (y_c-y)\cos\chi\} w_d, \tag{7}$$

where $\boldsymbol{x} := [x, y, \chi]^T$, $\boldsymbol{u} := [u, \tilde{u}]^T = [\sigma_c, \tilde{u}]^T$, w_c, w_u, w_r and w_d are weighting parameters, (x_c, y_c) and a are the center and the radius of the circular reference path respectively.

The terminal cost ϕ_J and the first term of L_J correspond to the distance between the SSRV position and the reference circle. Note that the dummy input $\tilde{u}$ appears only in the quadratic form in the constraint (5). Thus the term $-\tilde{u}w_r$ is added in (7) with a small positive constant w_r in order to make $\tilde{u}$ positive. If this term does not exist, the solution of $F = 0$ may not be unique and therefore the update of C/GMRES method may fail (Ohtsuka [2004]).

The last term in (7) is the cross product of the vehicle's ground speed vector and the vehicle's relative position from the center of the reference circle (x_c, y_c). The sign of w_d in this term determines from which side SSRV approaches the circle and this implies the direction of the circular motion of SSRV.

3.3 Steady wind velocity estimation

Among the variables of SSRV's equations of motion in Section 3.1, W_x, W_y and χ, which is calculated using true airspeed, cannot be measured directly from the sensor system. In order to calculate wind velocities from sensor data, angles of attack (α) and sideslip (β), as well as dynamic pressure, are in general essential. Although α and β can be measured by an air data sensor, they are sometimes inaccurate. In this paper the guidance law using MPC is realized without using α and β by utilizing an extended Kalman filter which estimates steady wind velocities and some of the state variables.

Here the following assumptions are made:

- Outputs from the navigation system are accurate
- Measured thrust contains a bias error
- Aerodynamic model (i.e. aerodynamic coefficients) is reliable
- Measured airspeed, or dynamic pressure, is available

As is mentioned in Section 2, the Micro-GPS/INS integrated navigation system is assumed to be used for SSRV. As for aerodynamic model uncertainty, the drag coefficient error, which is dominant, can be compensated by the bias error of the thrust. Thus these assumptions are reasonable.

State equations for extended Kalman filter State variables to be estimated are denoted by

$$\boldsymbol{x}_f = (V_T, \gamma, \chi, W_x, W_y, W_z, b_T),$$

where γ is a flight path angle calculated using the true airspeed, W_z is a wind velocity along z axis in the runway coordinate, b_T is a bias error of the measured engine thrust T. The state equation for $\boldsymbol{x}_f$ is denoted by

$$\dot{\boldsymbol{x}}_f = f(\boldsymbol{x}_f, \boldsymbol{u}_d, \boldsymbol{\eta}), \tag{8}$$

where $\boldsymbol{u}_d := (\phi, \theta, \psi, T_m)$ is a known control input vector; roll angle, pitch angle, yaw angle and measured engine thrust ($T_m = T + b_T$) respectively. The vector $\boldsymbol{\eta}$ is composed of process noises η_* in the equations below. These noises are assumed Gaussian-distributed.

The concrete form of the equation (8) is as follows (see Etkin [1982] for example):

$$\begin{aligned}
\dot{V}_T &= \frac{1}{m}[-D - mg\sin\gamma + (T_m - b_T)\cos\beta\cos\alpha] \\
\dot{\gamma} &= \frac{1}{mV_T}[(L + (T_m - b_T)\sin\alpha)\cos\sigma \\
&\quad + (-C + (T_m - b_T)\sin\beta\cos\alpha)\sin\sigma - mg\cos\gamma] \\
\dot{\chi} &= \frac{1}{mV_T\cos\gamma}[(L + (T_m - b_T)\sin\alpha)\sin\sigma \\
&\quad + (C - (T_m - b_T)\sin\beta\cos\alpha)\cos\sigma] \\
\dot{W}_x &= \eta_{w_x}, \quad \dot{W}_y = \eta_{w_y}, \quad \dot{W}_z = \eta_{w_z}, \quad \dot{b}_T = \eta_{b_T}.
\end{aligned}$$

In these equations, D, L, C are aerodynamic forces in the wind axis system defined as:

$$\begin{aligned}
D &= \frac{1}{2}\rho V_T^2 S(C_D(\alpha,\beta) + \eta_{c_d}) \\
L &= \frac{1}{2}\rho V_T^2 S(C_L(\alpha,\beta) + \eta_{c_l}) \\
C &= \frac{1}{2}\rho V_T^2 S(C_C(\alpha,\beta) + \eta_{c_c}),
\end{aligned}$$

where ρ is an air density, S is a reference area and $C_*(\alpha,\beta)$ is a dimensionless aerodynamic coefficients. As mentioned above, α and β are not available here (and neither is σ), but these can be regarded as functions of state variables γ, χ and known control inputs ϕ, θ, ψ.

Observation equations for extended Kalman filter Let

$$\boldsymbol{z}_f := (A_{X_m}, A_{Y_m}, A_{Z_m}, V_{ex_m}, V_{ey_m}, V_{ez_m}, V_{T_m}),$$

where A_{*_m} is a measured acceleration for each axis, V_{e*_m} is a measured ground speed for each axis in the runway coordinate and V_{T_m} is a measured airspeed. The observation equation is denoted by

$$\boldsymbol{z}_f = h(\boldsymbol{x}_f, \boldsymbol{u}_d) + \boldsymbol{\xi}, \tag{9}$$

where $\boldsymbol{\xi}$ is a vector composed of process noises ξ_* in the equations below. These noises are assumed Gaussian-distributed.

The concrete form of the equation (9) is as follows:

$$\begin{aligned}
A_{X_m} &= \frac{1}{m}(-D\cos\alpha\cos\beta - C\cos\alpha\sin\beta + L\sin\alpha \\
&\quad +(T_m - b_T)) + \xi_{ax} \\
A_{Y_m} &= \frac{1}{m}(-D\sin\beta + C\cos\beta) + \xi_{ay} \\
A_{Z_m} &= \frac{1}{m}(-D\sin\alpha\cos\beta - C\sin\alpha\sin\beta - L\cos\alpha) \\
&\quad +\xi_{az} \\
V_{ex_m} &= V_T\cos\gamma\cos\chi + W_x + \xi_{ex} \\
V_{ey_m} &= V_T\cos\gamma\sin\chi + W_y + \xi_{ey} \\
V_{ez_m} &= -V_T\sin\gamma + W_z + \xi_{ez} \\
V_{T_m} &= V_T + \xi_{vt}
\end{aligned}$$

Discrete-time predict and update equations Linearize the equations (8) and (9) online around the current estimated state for each estimation step, and then discretize them by the method in Brown and Hwang [1997]:

$$\begin{aligned}
\boldsymbol{x}_{f\,(k+1)} &= \Phi_{(k)}\boldsymbol{x}_{f\,(k)} + \boldsymbol{w}_{(k)} \\
\boldsymbol{z}_{f\,(k)} &= H_{(k)}\boldsymbol{x}_{f\,(k)} + \boldsymbol{v}_{(k)}
\end{aligned}$$

An estimated value of $\boldsymbol{x}_f$ and covariance matrix P are predicted and updated by the following steps (Brown and Hwang [1997]):

1. Update the Kalman gain $K_{(k)}$
$$K_{(k)} = P^-_{(k)}H^T_{(k)}(H_{(k)}P^-_{(k)}H^T_{(k)} + R)^{-1}$$
where $P^-_{(k)}$ is the covariance estimate predicted at the previous time step.
2. Update the state estimate $\hat{\boldsymbol{x}}_{f_{(k)}}$ using the measurement value $\boldsymbol{z}_{f\,(k)}$
$$\hat{\boldsymbol{x}}_{f_{(k)}} = \hat{\boldsymbol{x}}^-_{f_{(k)}} + K_{(k)}(\boldsymbol{z}_{f\,(k)} - H_{(k)}\hat{\boldsymbol{x}}^-_{f_{(k)}})$$
where $\hat{\boldsymbol{x}}^-_{f_{(k)}}$ is the state estimate predicted at the previous time step.
3. Update the covariance matrix $P_{(k)}$
$$P_{(k)} = (I - K_{(k)}H_{(k)})^T P^-_{(k)}$$
4. Predict the next estimate
$$\hat{\boldsymbol{x}}^-_{f_{(k+1)}} = \Phi_{(k)}\hat{\boldsymbol{x}}_{f_{(k)}}, P^-_{(k+1)} = \Phi_{(k)}P_{(k)}\Phi^T_{(k)} + Q$$
5. Go back to step 1

In these steps R and Q are covariance matrices of $\boldsymbol{v}$ and $\boldsymbol{w}$ respectively. These are adjustable parameters; R is tuned so that the estimation converges better through simulations and Q is set in accordance with the accuracy of sensors.

Among the estimated state $\hat{\boldsymbol{x}}_{f_{(k)}}$, χ is used in the nonlinear MPC calculation as an initial value in the prediction horizon. W_x and W_y are also used under the assumption that these are constant during the prediction horizon $T_s(t)$ sec. Other estimated states are used in other guidance and control systems (attitude control, for example).

Table 1. Maximum values of optimization error $||F||$ for each w_c.

w_c	10	100	500
Max. $\|\|F\|\|$	6.01×10^{-3}	6.13×10^{-3}	2.75×10^{-1}

4. SIMULATION

To evaluate the proposed guidance law, simulations were conducted using the simple lateral model of SSRV in Section 3.1. The sampling interval of the guidance law is 0.02 sec, the duration of the prediction horizon is defined as $T_s(t) := 10 \cdot (1 - e^{-0.1t})$, the number of grid points of the prediction horizon is $N = 10$, and the maximum and minimum bank angle commands are $\sigma_{\max} = +30$ deg and $\sigma_{\min} = -30$ deg respectively. The airspeed is assumed to keep constant value $V_T = 25$ m/sec.

Weighting parameters for the input u and dummy input $\tilde{u}$ are set as $w_u = 1$ and $w_r = 0.001$ respectively. The parameter w_d, which implies the direction of the circular motion of SSRV, is set as $w_d = -1$. This corresponds to the clockwise rotation from the top. It should be noted that, in order to balance the order of each term in ϕ_J and L_J, the unit of the position (that is, x, y, x_c, y_c and a) is converted to km when the cost functions of (6) and (7) are calculated.

Fig. 2 shows the simulation results [1] for three values of the weighting parameter w_c, which is critical for path following since it corresponds to the distance from the pre-specified reference circle. Each simulation starts from the position $(x, y) = (-100, -300)$. The center and the radius of the reference circle are $(x_c, y_c) = (100, 100)$ and $a = 300$. Due to the terms corresponding to w_u, w_r and w_d in the cost function L_J, a path-following error becomes larger with a smaller w_c. On the other hand, a larger w_c may make optimization in MPC calculation more difficult. Table 1 shows the maximum values of optimization error $||F||$ during simulations for each case. The maximum error of $w_c = 500$ is far larger than others, which means that the risk of onboard optimization failure is rather high. Therefore, in order to conduct flight tests safely, the weighting parameter w_c in the flight tests of SSRV is set as $w_c = 100$ with an allowable path-following error of around 10 m.

5. FLIGHT TESTS

This section describes flight test results of SSRV using the proposed lateral guidance law in Section 3.

[1] Note that the Y axis is in reverse direction because the positive Z axis points into the paper.

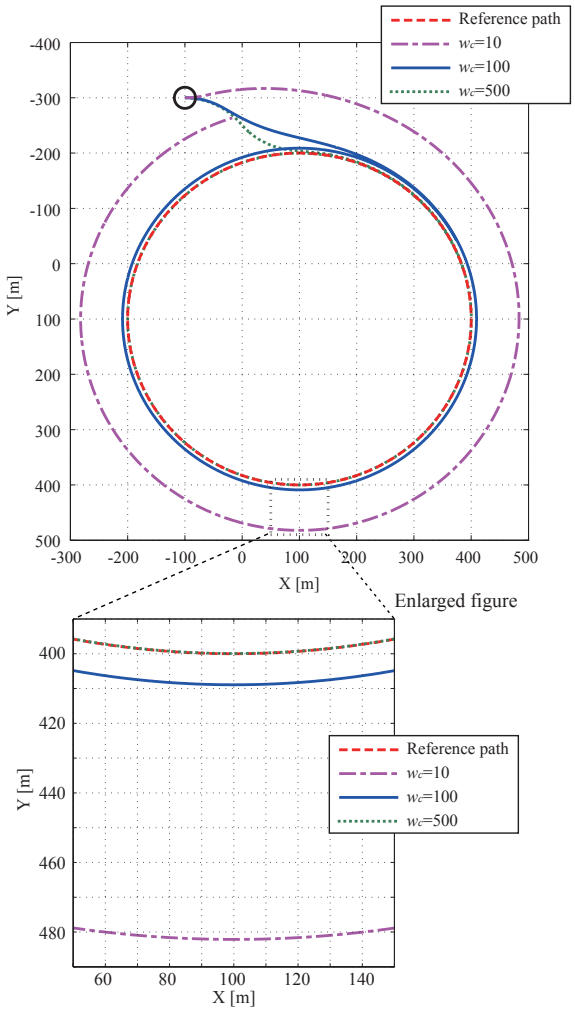

Fig. 2. Top: simulation results for $w_c = 10$ (broken line), $w_c = 100$ (solid line) and $w_c = 500$ (dotted line). Bottom: the enlarged figure.

Fig. 3. SSRV touchdown.

5.1 Overview of the flight tests

The flight tests were carried out in October 2012 at Taiki Aerospace Research Field in Hokkaido, Japan. 17 flights were conducted in total and each flight was proceeded in the following way:

- SSRV takes off. It is remotely controlled by an UAV pilot.
- After checking the flight condition, the pilot switches the control mode to automatic control.
- SSRV flight test is conducted with implemented automatic guidance and control system.

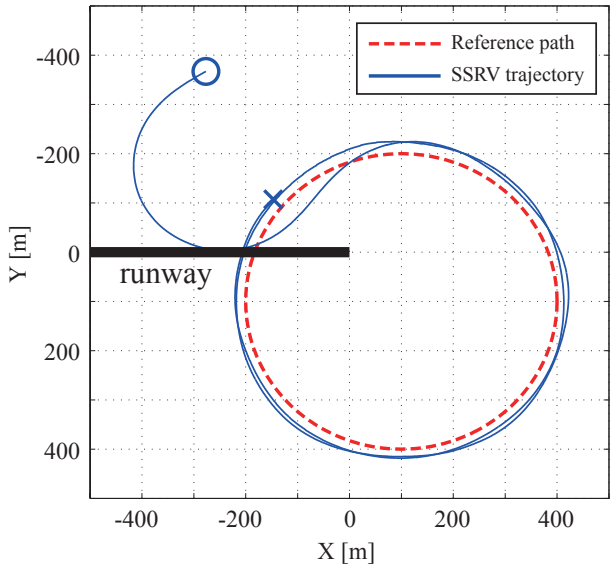

Fig. 4. The X-Y plot of the flight test using the nonlinear MPC. Broken line: circular reference path. Solid line: SSRV trajectory. ○: starting point. ×: end point.

- After finishing the test, the control mode is switched to return-to-base mode.
- When SSRV comes back into the area where the pilot can control, the control mode is switched to pilot control again.
- SSRV lands on the runway under pilot control (Fig. 3).

Although straight path following flight tests were also conducted, this paper shows only circular path following results. The weighting parameter w_c was set to 100 in flight tests and all other parameter values were the same as in Section 4. The airspeed was controlled by the longitudinal guidance system so as to keep constant.

5.2 Flight test results using the proposed method

Fig. 4 shows the trajectory of SSRV in X-Y plane using the proposed guidance law. Fig. 5 displays the time histories of X position, Y position, bank command σ_c and MPC optimization error $||F||$ during the flight test. SSRV started the flight test at a distant point from the circular reference path and approached to the circle with the minimum bank angle command in order to achieve the clockwise circular motion. During the flight test, the average wind velocity estimated onboard was $(W_x, W_y)_{ave} = (-2.3, -3.0)$. In spite of the wind, the center of the SSRV trajectory almost corresponded to the center of the circle $(x_c, y_c) = (-100, -300)$.

The magnitude of the optimization error $||F||$ is larger than that of the simulation result in Section 4. One of the reasons is because the onboard computer which carried out MPC calculation during the flight test was different from that used in the simulation. The important point here is that the error remained stable and it means MPC calculation was performed steadily.

The path-following error in the flight was about 15m, which is larger than that in the simulation. Recall that the simulation in Section 4 was conducted with quite a simple

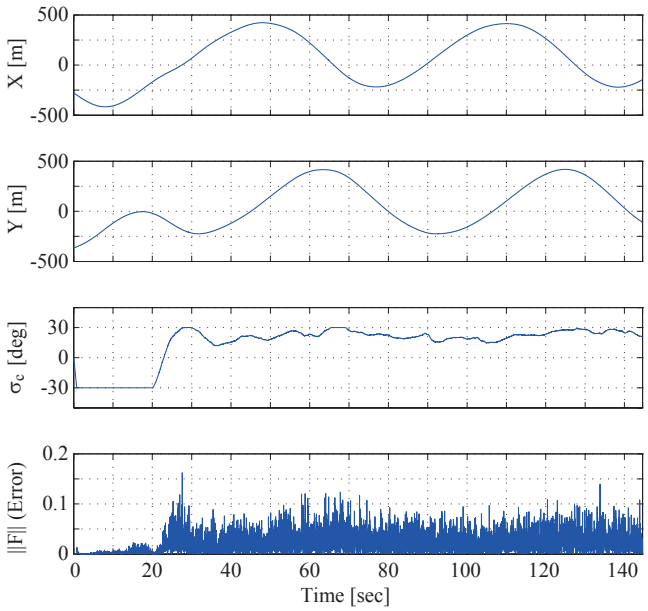

Fig. 5. The time histories of X-Y position, bank command and optimization error $||F||$ in the flight test.

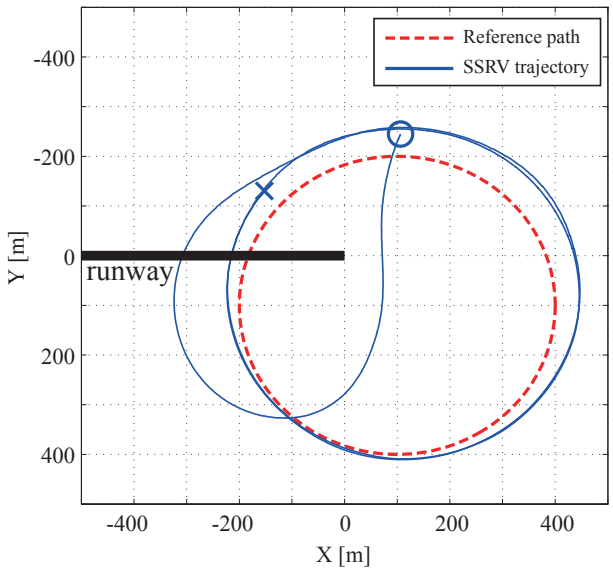

Fig. 6. The X-Y plot of the flight test using the nonlinear MPC without steady wind velocity estimation. Broken line: circular reference path. Solid line: SSRV trajectory. ○: starting point. ×: end point.

lateral model (i.e. equations (1)–(3)) under the nominal condition. In contrast, attitude control and longitudinal guidance were implemented as well as lateral guidance in the flight test. Thus the path-following error became larger due to interference by other guidance and control systems and some uncertainties.

5.3 Comparison with the flight test without steady wind velocity estimation

The flight test using nonlinear MPC without steady wind information was also conducted in order to show the importance of the wind velocity estimation. Fig. 6 is the flight result with $W_x = W_y = 0$ in the prediction model of MPC calculation. Apparently the center of the SSRV trajectory did not correspond to the center of the circle (x_c, y_c). Considering the fact that the average wind velocity estimated onboard during this flight was $(W_x, W_y)_{ave} = (3.2, -5.0)$, it seems that SSRV was drifted by the wind and the guidance law could not resist it. Therefore it is concluded that the extended Kalman filter for steady wind velocity information is crucial for precise lateral guidance.

6. CONCLUSION

The novel lateral guidance law was proposed based on nonlinear MPC using C/GMRES method. Since the proposed law is accompanied with the extended Kalman filter which estimates steady wind velocities, it is easy to follow a pre-specified reference path defined in a ground-fixed coordinate. The guidance performance was demonstrated by flight tests for circular path following using SSRV.

Although the guidance law was proved effective in lateral guidance, this is not sufficient for an orbital spaceplane. The next step is to extend the guidance law to longitudinal motion including altitude and velocity guidance. Add to that, an application to a vehicle that changes its dynamic characteristics during flight is also necessary in order to cover wide flight envelopes.

REFERENCES

R. G. Brown and P. Y. C. Hwang. *Introduction to Random Signals and Applied Kalman Filtering.* Wiley, 1997.

B. Etkin. *Dynamics of Flight: Stability and Control.* Wiley, 1982.

Y. Hamada, T. Tsukamoto, and S. Ishimoto. Lateral guidance of the small scale research vehicle by model predictive control – flight test results of straight trajectory tracking –. *SICE Journal of Control, Measurement, and System Integration (in Japanese)*, 50(3):236–244, 2014.

J. Kawaguchi and Y. Miyazawa. Flight control law design with hierarchy-structured dynamic inversion approach. In *AIAA Guidance, Navigation and Control Conference and Exhibit*, pages AIAA 2008–6959, 2008.

J. M. Maciejowski. *Predictive Control with Constraints.* Prentice Hall, 2002.

T. E. Moore. Space shuttle entry terminal area energy management. *NASA Technical Memorandum*, NASA-TM-104744, 1991.

NAL/NASDA HOPE Team. High speed flight demonstration (hsfd) phase 2. *JAXA Research Report*, JAXA-RR-04-026, 2005.

NAL/NASDA HSFD1 Team. Results of high speed flight demonstration (hsfd) phase 1 flight experiment. *JAXA Research Report*, JAXA-RR-03-011, 2004.

T. Ohtsuka. A continuation/gmres method for fast computation of nonlinear receding horizon control. *Automatica*, 40(4):563–574, 2004.

M. Shirouzu, S. Ishimoto, Y. Miyazawa, and M. Yanagihara. Development of hope-x and high speed flight experiment. *NAL Research Progress 1998–2000*, pages 8–11, 2001.